Does cell polarization matter in single-ion conducting electrolytes?

Kristina Borzutzki[†], Jijeesh Ravi Nair[†], Martin Winter^{†,‡}, and Gunther Brunklaus^{†,*}

KEYWORDS Lithium metal battery, Single-ion conducting polymer electrolyte, Lithium electrolyte interphase, polariasation, Chazalviel model, limiting current density

ABSTRACT: Single-ion conducting polymer electrolytes (SIPE) are particularly promising electrolyte materials in lithium metal-based batteries (LMBs) since theoretical considerations suggest that the immobilization of anions avoids polarization phenomena at electrode|electrolyte interfaces. SIPE in principle could allow for fast charging while preventing cell failure induced by short circuits arising from the growth of inhomogeneous Li depositions provided that SIPE membranes possess sufficient mechanical stability. To date, different chemical structures are developed for SIPE where new compounds are often reported through electrochemical characterization at low current rates. Experimental counterparts to model-based assumptions and determination of system limitations by correlating both, models and experiments, are rare in literature. Herein, Chazalviel's model which is derived from ion concentration gradients is applied to theoretically determine the limiting current density (J_{Lim}) of a SIPE. Comparison to the experimentally obtained J_{Lim} reveals a large deviation between the theoretical and practical values. Beyond that, charge-discharge profiles show distinct arcing behaviour at moderate current densities (0.5 mA cm⁻² to 1 mA cm⁻²) indicating polarization of the cell, which is not so far reported for SIPEs. In this context, by application of various electrochemical and physiochemical methods the details of cell polarization and the role of the SEI in producing arcing behaviour in the voltage profiles in stripping/plating experiments is revealed which eventually also elucidates the inconsistency of J_{Lim} .

1. INTRODUCTION

Significant enhancement in energy density of rechargeable batteries is required to fulfil the demands for new application fields such as electric vehicles and futuristic electronic devices. Current research strongly focuses on the development of so called "post lithium -ion battery" (LIB) technologies¹, which might replace common graphitic anode materials (specific capacity of 339 mAh·g⁻¹ in the lithiated (charged) state) by lithium metal anodes (theoretical capacity 3860 mAh·g⁻¹).^{2,3} Lithium metal is often incompatible with conventional liquid electrolytes as inhomogeneous, high-surface area lithium metal (HSAL) deposits are eventually formed that could induce cell short circuit by piercing the separator⁴. In view of their superior mechanical properties and customizable chemistry, polymer electrolytes are considered essential to significantly suppress formation of dendritic lithium or HSAL deposits, while providing appropriate flexibility to allow for sufficient interfacial contacts towards the electrodes that are required to fully exploit fast charging protocols relevant for industrial applications. 5-7

Single-ion conducting polymer electrolytes (SIPEs) with immobilized anions and solely Li⁺ ions as mobile species constitute an attractive material class since theoretical investigations by J.-N. Chazalviel conducted on dual-ion conducting systems revealed that the growth of dendritic lithium metal correlates with depletion of anions at the negative electrode at sufficiently high current densities.⁸

Notably, an important quantity derived from Chazalviel's model comprises the limiting current density (J_{Lim}) , defined as the minimum current density at which anion depletion likely occurs at the negative electrode. Below J_{Lim} , concentration gradients generated within electrolytes do not induce local depletion of anions, rendering the growth of dendritic lithium structures and occurrence of cell short circuit highly unlikely. Considering that $J_{Lim} \sim \frac{1}{t_a}$, with t_a being the transference number of the anion, immobilization of anionic moieties $(t_a \rightarrow 0, t_{Li+} \rightarrow$ 1) constitutes a versatile approach to prevent cell polarization thereby improving the achievable rate performance of cells.^{8,9} While J_{Lim} is a critical quantity to evaluate the performance and applicability of electrolytes, though few experimental studies, mainly dedicated to liquid-based electrolytes, include valid experimental measurements of this relevant parameter. 10-12 Note, however, that Chazalviel's model is a simplified representation derived for ideal dilute solutions unlike most actually applied concentrated electrolytes. Nevertheless, for PEO/LiTFSI systems, it was demonstrated that the model predictions are in good agreement with the electrochemically obtained values for J_{Lim} , illustrating that Chazalviel's model can be sufficiently accurate even in case of non-ideal electrolytes. 13 Therefore, it is recommended to readily exploit Chazalaviel's model for newly developed electrolyte compounds to achieve first impressions of

[†]Helmholtz-Institute Münster, IEK-12, Forschungszentrum Jülich, Corrensstr. 46, 48149 Münster, Germany

[‡] University of Münster, MEET Battery Research Center, Institute of Physical Chemistry, Corrensstr. 46, 48149 Münster, Germany

likely achievable electrochemical performances and system limitations.

Current research efforts mainly report the development of novel synthesis routes and polymer design strategies (e.g. introduction of tailored functional groups, anionic moieties monomeric units or polymer blocks thereby e.g. improving the yield or simplicity of the synthesis while enhancing mechanical and/or Li⁺ ion transport properties). 14-17 This way, various new (single-ion conducting) polymer structures are introduced where basic characterizations and cycling investigations are done under mild conditions aiming at demonstrating a general applicability/acceptability of these compounds as electrolytes. 18-20 Experimental studies of limiting conditions or correlations with respect to reliable model predictions are quite rare so far,²¹ despite that insights derived from such analyses are essential to unravel internal electrochemical or physical processes and mechanisms. The latter in turn could allow for the development of both tailored and generic routes to achieve enhanced overall cell performances.

Beyond that, gaining insights into the interphases, specifically the solid electrolyte interphase (SEI²²) composition is fundamental to understand electrochemical processes, in particular during cell cycling.²³⁻²⁵ Interphasial characteristics and phenomena, including details of electrochemical Li metal deposition and correlations thereof in the case of polymers, specifically salt-free SIPEs (where anionic moieties are immobilized by attachment to the polymer structure), are not yet fully understood. However, profound studies on liquid electrolyte-based LMBs emphasize the substantial impact of SEI characteristics (such as e.g., chemical composition, thickness, flexibility and homogeneity) on the actual Li metal deposition behaviour and cycling performance (longevity, interphase resistance). 26,27 It has to be especially regarded, that interphase formation by electrolyte decomposition usually involves decomposition of all electrolyte constituents, i.e. solvent(s), additive(s) and salt anions. In case of SIPE, the immobile anions thus cannot contribute sustainably to interphase formation and interphase composition. Nevertheless, previous studies on dual-ion conducting electrolytes revealed that, among several other factors, e.g. cycling conditions, electrolyte solvents or additives that are utilized, ^{27,28} particularly the lithium salt and corresponding decomposition products, were identified to substantially dominate the formation of SEI layers, explicitly, the presence of specific moieties of different salt chemistries (e.g., boron containing LiBF4 or fluorine containing LiN(SO₂CF₃)₂) as well as salt concentrations define both the SEI thickness and composition. 29-31 In this work, the behaviour of a well-characterized quasi-solid blendtype SIPE membrane in symmetric Li cells at elevated current densities and corresponding interphase relations are explored. Chazalviel's model is consulted as mathematical framework for determination of J_{Lim} and subsequent comparison to experimentally obtained data. It is observed that the predicted and experimentally established values strongly deviate. In addition, significant polarization effects occur in the electrochemical experiments already at moderate current densities well below J_{Lim} in stark contrast to the common believe that SIPE should substantially diminish or even avoid cell polarization. 16-18 Applying a combination of various electrochemical protocols³² and correlating these results to spectroscopic techniques the critical role of SEI composition for Li⁺ ion transport is revealed. It is illustrated that the application of high current rates results in cell

polarization, since limited Li⁺ ion diffusion through SEI impairs the actual rates of charge transfer and achievable current densities upon cell operation (fast charging conditions) more significantly than charge transport properties of the bulk polymers themselves.

2. EXPERIMENTAL

SIPE synthesis and fabrication of the blend polymer membrane were performed following reported protocols.³³ The blend polymer membranes composed of 75 wt% SIPE and 25 wt% PVdF-HFP were prepared by solution casting and subsequent drying. The membranes were then punched to 14 mm disks and subsequently soaked in a mixture of ethylene carbonate (EC) and propylene carbonate (PC) (1:1, v: v) for 24 hours yielding well functional, non-tacky and self-standing SIPE membranes.

Lithium metal (500 µm, Albemarle, Germany) was roll pressed prior to cell assembly to achieve defined, flat, defect free electrode surfaces. Strips of Li metal (\sim 10 cm) were placed between two siliconized polyester foils (PPI Adhesive Products Ltd) and pressed in a table top roll press (Hohsen Corp., HSAM-615H) thereby reducing thickness in 25 µm steps to a final thickness of 300 µm. Li metal electrodes of 12 mm diameter were then punched from the Li stripe.

Electrochemical investigations were conducted at 60 °C in Li||Li cells (CR2032 coin cells) either on a battery analysis system Maccor 4000 (USA) in case of galvanostatic cycling or on a potentiostat (VMP3, Bio-Logic Science Instruments) in case of combined galvanostatic cycling and electrochemical impedance spectroscopy (EIS) measurements. EIS was conducted by applying an alternating voltage of 10 mV in a frequency range between 1 mHz and 1 MHz. All cells were kept at open-circuit voltage (OCV) for 12 hours prior to cycling.

Changes in the chemical composition of SIPE were determined by spectroscopic methods. ¹H liquid NMR spectra were recorded at a BRUKER 400 AVANCE III HD instrument at 293 K, where deuterated dimethyl sulfoxide (DMSO-d6) was used as reference signal for the ¹H spectra.

In addition, attenuated total reflection Fourier transform infrared spectroscopy (ATR FTIR) was performed on the device: Bruker Vertex 70 in a spectral range between 400 cm⁻¹ and 4000 cm⁻¹, a spectral resolution of 1 cm⁻¹.

The SEI composition was analysed by X-ray photoelectron spectroscopy (XPS) with an AXIS Ultra DLD (Krato). For the measurements, a monochromatic Al K α source (hf = 1486.6 eV), 10 mA filament current and 12 kV filament voltage source energy were utilized. To avoid charging of the sample a charge neutralizer was exploited. A 0° angle of emission and a pass energy of 20 eV were applied. A 0° angle were prepared in a dry room (H2O < 20 ppm, dew point below -65 °C) and transferred to the XPS device without exposure to ambient atmosphere. For each sample, three measurements were performed at different spots; resulting spectra were fitted with the software, *CasaXPS*, where the binding energy of the C-C/C-H peaks of the C 1s spectra was set to 284.6 eV for calibration.

3. RESULTS AND DISCUSSION

3.1 Theoretical and experimental determination of limiting current density

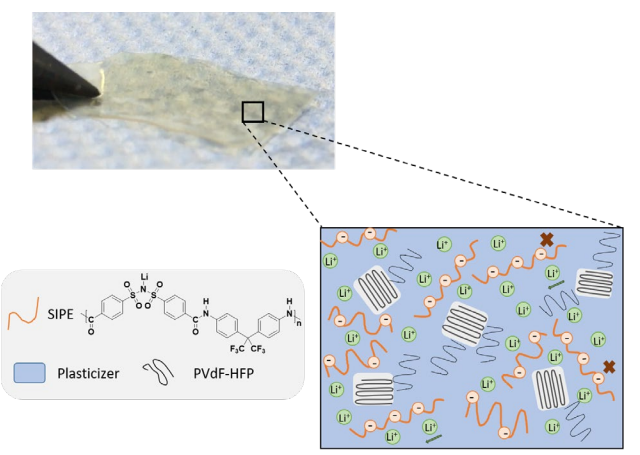


Figure 1 Image and scheme of the investigated single-ion conducting polymer membrane. The red cross in the scheme indicates the immobility of the anionic species whereas the blue arrow indicates the mobility of Li+ ions.

Table 1 Properties of the SIPE membrane applied for the determination of the limiting current density.

Membrane geometry	
Membrane thickness/ electrode distance	80 μm
Weight of the dry membrane	10 mg
Solvent uptake	130 wt% (ref. ³³)
Transport properties of the	Value at 60 °C
membrane	
membrane Ionic conductivity	1.08 mS cm ⁻¹ (ref. ³³)
	1.08 mS cm ⁻¹ (ref. ³³) 3.08 ×10 ⁻¹¹ m ² s ⁻¹ (ref. ³³)
Ionic conductivity	
Ionic conductivity Li ion diffusion coefficient	3.08 ×10 ⁻¹¹ m ² s ⁻¹ (ref. ³³)

The considered SIPE comprises aromatic single-ion conducting constituents and a flexible linear polymer (poly(vinylidene difluoride-co-hexafluoropropylene), PVdF-HFP) in a ratio of 3:1 (wt%:wt%) as well as carbonate-based plasticizers (EC: PC, 1:1 by volume). In Figure 1 an image of the self- standing blend membrane and a schematic of its composition are presented. The polymer membrane yields outstanding ion transport properties (Table 1), including an ionic conductivity of 1 mS cm⁻¹ at 60 °C, ion diffusivity of $D_{\text{Li}^+} \approx 10^{-11} \,\text{m}^2\text{s}^{-1}$, single-ion conducting behaviour ($t_{+,Li} = 0.9$) and is applicable in NMC || Li and LFP|| Li cells at 60 °C and 20 °C as demonstrated in our previous works. 33,36,37 For this well-characterized membrane, the applicability and cycling behaviour at elevated current rates will be studied. The theoretically predicted short circuit time $J_{Lim\ theo}$ is determined based on Chazalviel's model and subsequently correlated to experimentally obtained data. J_{Lim theo}can be expressed as³⁸

$$J_{Lim\ theo} = \frac{2eC_0D}{t_aL} \tag{1}$$

where c_0 is the initial Li⁺ ion concentration, e the elementary charge, t_a the anion transference number, L the distance between the electrodes and D the ambipolar diffusion coefficient that can be related to the D_{Li} + via

$$D_{Li^+} = \frac{D}{2*(1-t^+)} \tag{2}$$

with t^+ the Li ion transference number. The value obtained for the SIPE (properties inserted in equation 1 are summarized in Table 1) amounts to $J_{Lim\ theo} = 12\ \text{mA}\ \text{cm}^{-2}$.

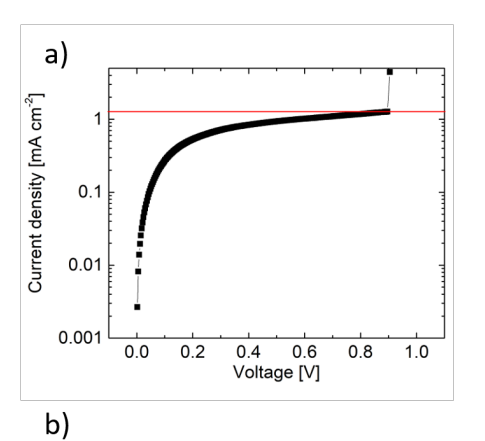
Experimental determination of $J_{Lim\ exp}$ was realized by linear sweep voltammetry (LSV, Figure 2a). Lithium dendrite penetration and likely cell short circuit was monitored when the current eventually increased from 1.3 mA cm⁻² to 4.5 mA cm⁻² thereby defining the threshold (or limiting) current density to 1.3 mA cm⁻² ($C = 14.8 \text{ C cm}^{-2}$). The resulting experimental value is in agreement with experimental values of about 1 mA cm⁻² that are recently reported for similar quasi-solid SIPEs equally determined by LSV.^{39,40}

Nonetheless, contrary to good agreements obtained between theory and experiments in PEO/LiTFSI-based systems¹³, in case of SIPE compounds the experimental result strongly deviates from $J_{Lim\ theo}$ of 12 mA cm⁻². The question of what causes these strong deviations and how J_{Lim} can be achieved in practice will be clarified in the following.

3.2 Combinatorial electrochemical and spectroscopic analyses of internal cell processes

To gain deeper insights into the underlying processes and reversibility of Lithium deposition/dissolution processes a stripping/plating procedure with stepwise increase in current density (here by 0.1 mA cm⁻²) with several cycles at the initially low current rate of 0.1 mA cm⁻² in between (Figure 2b) was performed. In this experiment, cell failure (a sudden decrease in the overvoltage; the magnified overvoltage profiles of Figure 2b are presented in Figure S1) occurs already at a lower current density of 0.7 mA cm⁻² compared to the LSV measurement which is reasonable as the SIPE membrane underwent several stripping/plating cycles and a substantially larger amount of charge of 192.2 C cm⁻² (compared to LSV experiments) was passed through the membrane thus inducing deformation and (mechanical) stress. Note, that even after cell failure (due to short circuit) the overvoltage changes when different current rates are applied (0.1/0.8/0.1 mA cm⁻²), which can be attributed to a non-zero resistance of dendritic Lithium metal.⁴¹

It is noticeable that the overvoltage in Figure 2b increases (non-linearly) with increasing current rate while almost reversibly reaching the initial value of 0.02 V for repeated cycles at 0.1 mA cm⁻² indicating minor changes in interfacial/interphasial resistance as well as surface area during repeated Lithium deposition. However, for consecutive cycles at current rates ≥ 0.4 mA cm⁻², the overvoltage increases with cycle number, limiting achievable cell performances. Identical behaviour was observed for a membrane composed of a 1:1 ratio of single-ion conducting polymer and PVdF-HFP, (instead of 3:1) by weight, (Figure S2) featuring a lower content of Li⁺ ions within the membrane, and consequently lower ion transport properties ($\sigma = 0.21$ mS cm⁻² and $D_{Li^+} = 0.91 \times 10^{-11}$ m²s⁻¹ at 60 °C).³³ This observation



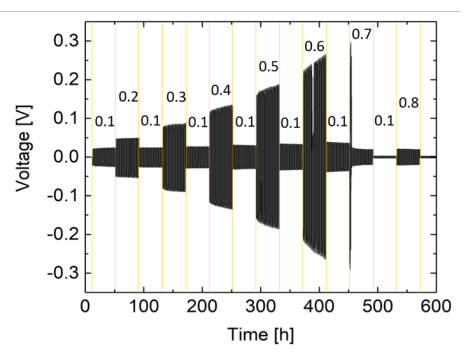


Figure 2 Cycling investigations in symmetric Li||Li cells. a) Current density-overvoltage curve for linear sweep voltammetry with a scan rate of $0.05~\text{mV}~\text{s}^{-1}$ and b) Stripping/plating investigation applying varying current densities as indicated by the numbers in the graph for 1 h per half cycle.

highlights that the progression of the overvoltage is independent of the SIPE transport properties.

To account for any decomposition products of the electrolyte, FTIR and ¹H NMR analysis were performed on fresh and cycled membranes (after 150 cycles at 0.2 mA cm⁻² or 5 cycles at 1 mA cm⁻² for 1 h, Figure S3 and S4).

Upon long term cycling, 1H NMR spectra confirm compositional changes of the solvent solution (EC: PC) (Figure S4). After 550 h of cycling at 0.2 mA cm⁻² with 2 h stripping/plating duration, the EC:PC ratio determined by integration of the corresponding signals (singlet at $\delta = 4.49$ ppm in case of EC and doublet at $\delta = 1.36$ ppm, triplets at $\delta = 4.90$ ppm, 4.57 ppm and 4.06 ppm for PC) is reduced from 1:1 (v: v) to 0.9:1 (v: v). Thus, based on their reductive stabilities, 42 EC consumption takes place prior to the consumption of PC for SEI formation as a consequence of continuous destruction upon Li stripping and plating. 43 However, no changes or additional peaks were observed, not even at an elevated current density of 1 mA cm⁻² (Figure S3), so that chemical decomposition of the polymer membrane was excluded as likely reason for the observed

increase in overvoltage at higher current densities, rendering this phenomenon correlated to electrochemical processes.

To reveal the underlying mechanisms of the observed trends in overvoltage, a combination of electrochemical methods was consulted, particularly galvanostatic cycling was performed for 6 cycles at various current densities whereby OCV, chronoamperometry (CA) and electrochemical impedance spectroscopy (EIS) were recorded in between every set of cycles. Figure 3a presents the overvoltage progression of this combinatorial stripping/plating experiment with 1h duration and 6 cycles each at: $0.05 \text{ mA cm}^{-2} (\triangleq 0.0115 \text{ mg Li}), 0.5 \text{ mA cm}^{-2} (\triangleq 0.115 \text{ mg Li}),$ 0.05 mA cm^{-2} , 1 mA cm⁻² ($\triangleq 0.23 \text{ mg Li}$) and again 0.05 mA cm^{-1} ². While the overvoltage at the low current density of 0.05 mA cm⁻² shows an almost rectangular shape and flat voltage plateau (as anticipated in a SIPE), increasing overvoltage (arcing behaviour) at higher current densities (0.5 mA cm⁻², 1 mA cm⁻²) occurs within every half-cycle, revealing that polarization phenomena are present in the cells, which represents an unexpected observation. (Similar behaviour can be seen in the overvoltage profiles of Figure 2b which are presented in detail in Figure S1.) The arcing behaviour is strongly pronounced at higher current rates (i.e. 1 mA cm⁻²), while it is only slightly visible at 0.5 mA cm⁻². As indicated in the extract in Figure 3a highlighting the cycles performed at 1 mA cm⁻² no plateau value was reached within the stripping/ plating duration of one hour whereas the overvoltage continuously increases from $V_1 = 348$ mV to $V_2 =$ 723 mV and from $V_3 = 359$ mV to $V_4 = 768$ mV.

Note, that arcing behaviour is also observed in e.g. a solid polymer/oxide single-ion conducting hybrid and a ceramic electrolyte, though underlying mechanisms were not investigated. 44,45

Moreover, as indicated by the dashed lines in the insert in Figure 3a, the overvoltage further increases with increasing cycle number ($V_1 = 348 \text{ mV to } V_5 = 497 \text{ mV}$). Cycles at 0.05 mA cm⁻ ² conducted in the beginning and in between the cycles at 0.5 mA cm⁻² and at 1 mA cm⁻² exhibit slightly increased overvoltages (16 mV (1), 18 mV (2), 23 mV (3)) reflecting the occurrence of minor irreversible processes, probably due to EC consumption and changes at the interphase. Note though, that while all trends discussed here are reproducible (a second cell showing reproducibility is presented in Figure S5), the explicit values of the overvoltages may vary within a certain range among cells fabricated in different batches; (e.g., at 1 mA cm⁻²: values of 240 - 380 mV are observed as initial overvoltage V_1 , V_3 , and 290 - 750 mV were recorded for V_2 , V_4 (Figure 3 and S5). Despite that roll pressing was performed, thereby breaking and partially removing native SEI layers of the Li metal surface,34 the impact of varying compositions of native SEIs related to different conditions of the Li foils (such as impurities, changes in the original lithium layer upon storage/ageing in the glove box, etc.) cannot be completely avoided. Similar observations of

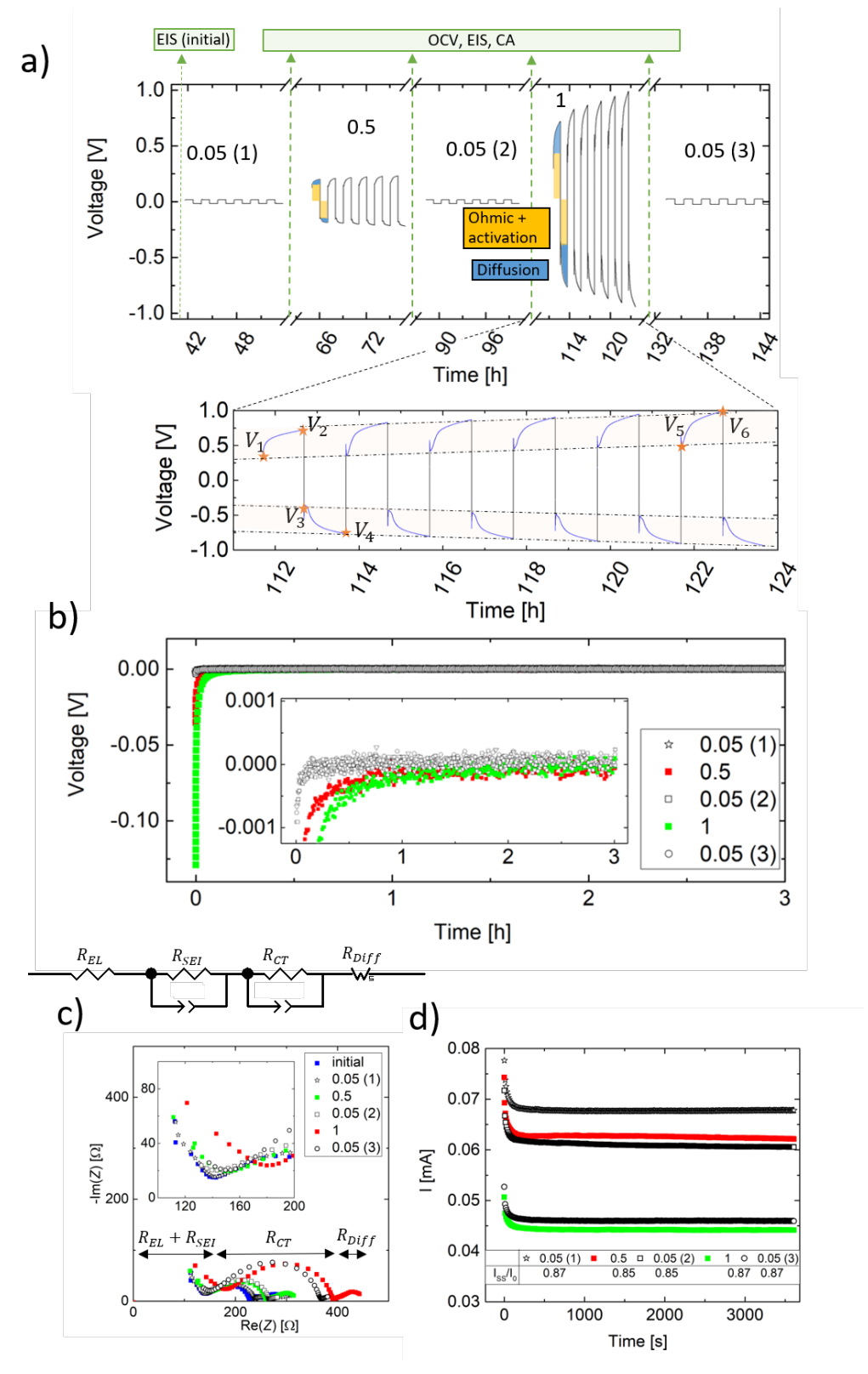


Figure 3 Electrochemical investigations applying procedures 1 and 2 after one another a-c) Procedure 1: a) Stripping/plating experiment applying different current densities as indicated by the number above the individual cycle b) OCV recorded directly after every 6 cycles of a) with varying current rates, c) EIS recorded after stripping/plating + OCV for every set of cycles.d) CA measurements performed within the cycling procedure.

strongly deviating overvoltages related to Li metal surface/SEI characteristics have also been reported for ceramic sulphide-based solid electrolytes.⁴⁴

To monitor the kinetics of the considered SIPE system while identifying origins of the observed polarization phenomena, after every cycling step, (6 cycles at varying current rates) OCV was recorded (Figure 3b) for 6 h followed by EIS (Figure 3c) and chronoamperometry (CA) (Figure 3d). The OCV curves show significant differences: the higher the applied current density, the longer it takes until equilibrium is reached. After cycling at 0.05 mA cm⁻², a constant voltage is observed after a few seconds, whereas it takes ≈ 120 min after cycling at 1 mA cm⁻². This relaxation-type behaviour verifies that charge separation is induced at higher current rates, as indicated by the progression of the overvoltage. Due to long relaxation processes (even longer than the duration of 1h of every half-cycle that was applied in the experiment), performing multiple cycles results in a constant increase of the initial overvoltage of each half cycle, even after switching the current direction ($V_1 = 348 \text{ mV}$, $V_3 =$ 386 mV, $V_5 = 497$ mV), since charges are still distributed nonuniformly within the system. The EIS spectra recorded after each stripping/plating step are fitted with equivalent circuit (Figure 3c) models including contributions from SIPE bulk electrolyte (El, R_{El}), the SIPE|Li interphase (Int, R_{SEI}), charge transfer processes (CT, R_{CT}) and diffusion related processes (DIFF). The latter is represented as a finite Warburg element (W_s) , valid for diffusion originating from a diffusion layer of finite thickness, thus indicating the presence of a blocked interphase. 46,47 The obtained resistances were then correlated to the overvoltages by roughly estimating the portions of overvoltage related to kinetic charge transfer (activation process related to the velocity of charge transfer at the electrode electrolyte interphases), diffusion, bulk electrolyte and interface resistances and a portion corresponding to polarization processes (Table 2).

Therefore, the overall resistance was multiplied with the current I = J * A, assuming a constant area of the Lithium electrodes. Note though, that W_S cannot be not fully covered by the accessible frequency range

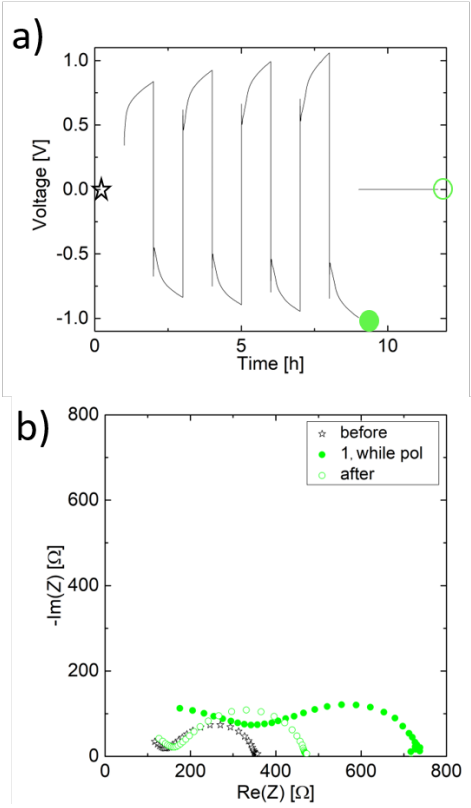


Figure 4 a) 4 cycles at 1 mA cm⁻² and b) EIS recorded before cycling (star symbol), while the final voltage is held (green circles, filled) and 6h after cycling (green circles, open)

Table 2 Resistances and overvoltages obtained from Figure 3 and 4. Combined electrolyte and SEI resistance ($R_{El} + R_{SEI}$), charge transfer resistance (R_{CT}), diffusion related resistance (R_{Diff}) determined by fitting the impedance spectra in Figure 2c and 2e and overvoltages V_1 and V_2 referring to the initial and final value of the corresponding half cycle and calculated overvoltages η_{calc} .

	J [mA cm ⁻²]	$R_{El+SEI}[\Omega]$	$R_{CT}\left[\Omega\right]$	$R_{Diff} [\Omega]^*$	<i>V</i> ₁ [mV]	V_2 [mV]	$\eta_{Calc} [ext{mV}]$
Exp 1	Initial	140 ± 3	88 ± 5	30 ± 5			
(E: 2)	0.05(1)	138 ± 3	87 ± 5	28 ± 10	15 ± 2	16 ± 2	15 ± 1
(Fig.3)	0.5	149 ± 3	113 ± 5	63 ± 10	136 ± 4	200 ± 2	143 ± 3
	0.05(2)	143 ± 3	124 ± 5	32 ± 10	17 ± 2	18 ± 2	18 ± 1
	1	161 ± 3	217 ± 5	68 ± 10	348 ± 10	723 ± 2	337 ± 6
	0.05(3)	153 ± 3	217 ± 5	32 ± 10	23 ± 2	24 ± 2	25 ± 1
Exp 2	Before pol	139 ± 3	215 ± 5				400 ± 6
(Fig.4)	1- while pol	389 ± 20	371 ± 20		403 ± 20	985 ± 10	$860 \pm 23 **$
(1 ¹ 1g.4)	After pol	159 ± 3	312±5				512 ± 6

^{*}Note that determination of R_{Diff} was rather inaccurate and in some cases not possible at all due to limited data points (caused by the limited frequency range of the device).

^{**}Underestimation of the calculated overvoltage as R_{Diff} was covered by the data points obtained by EIS and could thus not be considered.

of the measurement device and is thus determined with rather high uncertainty. Nevertheless, in case of spectra repeatedly recorded at 0.05 mA cm⁻², both the estimated and experimentally obtained values are in good agreement within < 10% deviation for all cases, confirming that the overvoltage recorded can be solely attributed to Ohmic resistances and the activation processes (related to CT, R_{CT}). For higher current rates of \geq 0.5 mA cm⁻² though, the estimated values agree well with the initial value recorded directly after application of the current (shown in orange in Figure 3a, e.g. V_1, V_3 and V_5). Consequently, the additional contributions of the overvoltage that increase with time (arc-like behaviour, coloured in blue in Figure 3a) can indeed be fully assigned to polarization overvoltage thus corroborating the previous assumptions.

It is noticeable that the fraction of the polarization overvoltage at 0.5 mA cm⁻² amounts to one quarter (25%) to the overall cell voltage while becoming the dominating process at 1 mA cm⁻² (53% of the overvoltage contribution). Based on the CA curves (Figure 3d) the transference number t^+ of the polymer membrane is estimated by a simplified expression⁴⁸ $t^+ = \frac{l_{ss}}{l_0}$ which can be considered sufficiently reasonable since EIS data

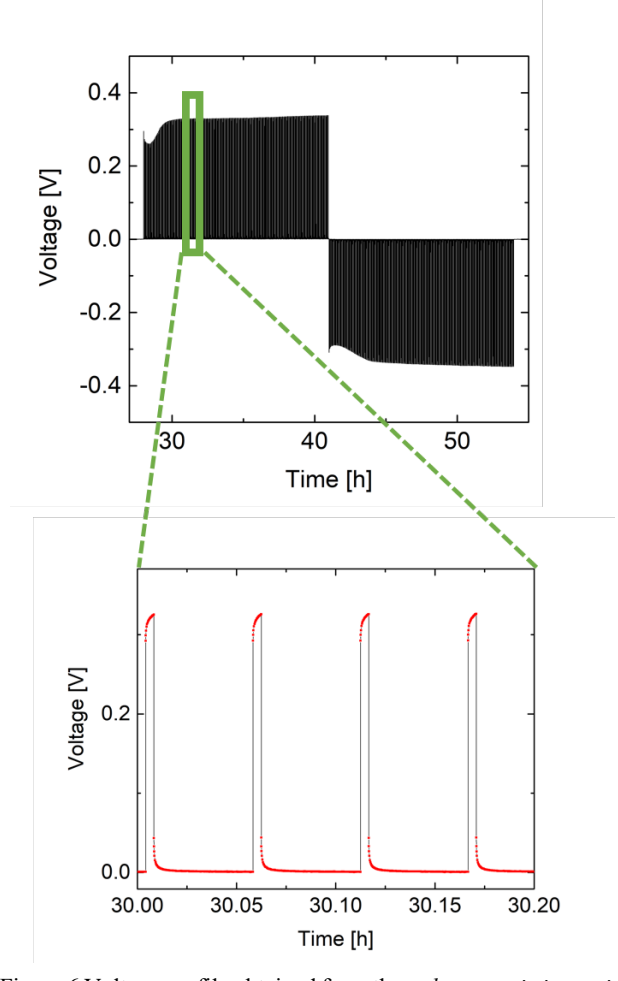


Figure 6 Voltage profile obtained from the *galvanostatic intermittent titration technique (GITT)* with 240 pulses of 1 mA cm⁻² for 15 seconds followed by a rest period of 3 minutes (equivalent charge transfer of C = 3.6 C cm⁻² as for the galvanostatic cycles at 1 mA cm⁻² for 1h).

in Figure 3c imply that the comparably small voltage applied during CA does not change the interfacial/interphasial resistances. The values for I_{ss}/I_0 remain constant $(t^+=0.9)$ throughout the experiments thereby illustrating that in agreement to both NMR and FTIR data (Figure S3) no decomposition that otherwise would release additional anionic species occurs. In contrast to model-based assumptions considering perfect single ion conductors with $t^{+}=1$, in the case of 'real' polymer electrolytes where t^+ values of 0.7-0.95 were reported, 15 small fractions of anionic species are present that most likely reflect minor decomposition of the polymer materials when being in contact with the Li metal. This fraction of anions may thus contribute to the build-up of concentration gradients and consequently cell polarization. Since an arcing behavior was not observed in case of lower current densities (e.g. 0.05- 0.1 mA cm⁻²) but appeared at higher current densities, anionic species are likely present in a 'bound state', e.g. as ion pairs, up to a certain threshold value of the current density where cations and anions both are dissociated.

After having performed an analysis presented in Figure 3, four additional cycles at 1 mA cm⁻² were applied to the cell and impedance spectra were recorded before application of a current (t = 0 h), when the polarization voltage was held (t = 9 h), and after an OCV period of 4 h (t = 13 h) (Figure 4). As the cell is under polarization, a significant increase in R_{EI} + R_{SEI} (from $139 \pm 3 \Omega$ to $389 \pm 20 \Omega$) as well as in R_{CT} (from

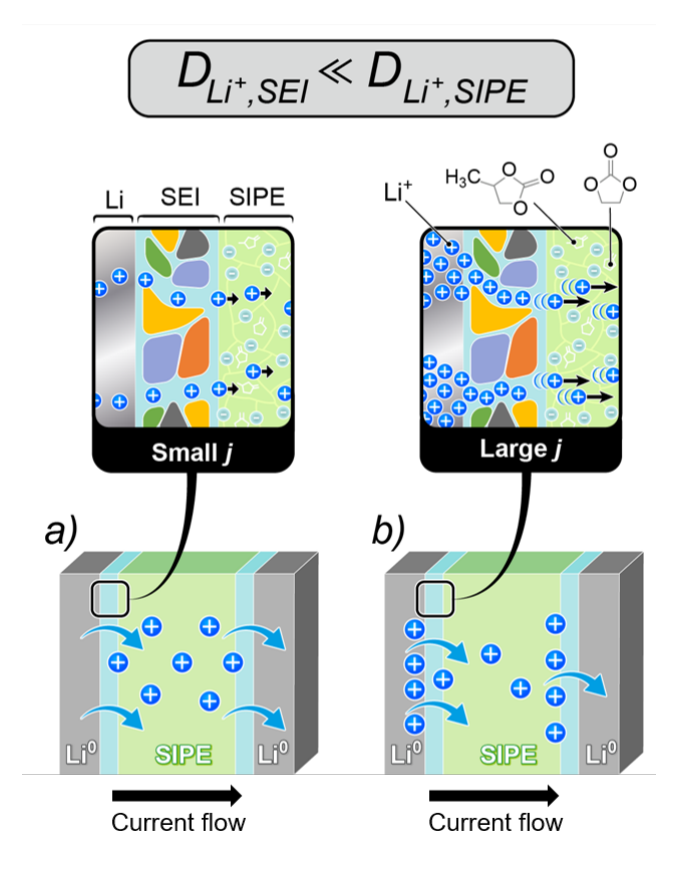


Figure 5 Schematic presentation of the Li ion concentration distribution in a symmetric Li||Li cell in case that Li+ diffusivity of the SEI layers represents the kinetically limiting factor for Li ion transport. a) Application of small current densities b) application of high current densities.

 $215 \pm 5 \Omega$ to $371 \pm 20 \Omega$) (Table 2) is observed, which agrees with the presence of finite Warburg elements (blocking interphases) and supports the conclusion that polarization within the cell is generated by interphases. After an additional OCV time of 6h, allowing the system to return to equilibrium, $R_{El} + R_{SEI}$ almost reversibly approaches its initial value whereas R_{CT} is still noteworthy increased (312 Ω) compared to the value prior to cycling-likely related to the decomposition of plasticizer molecules. The galvanostatic intermittent titration technique can be used as analytical method that limits the impact of polarization in Li||Li cells49-52 since intermittent relaxation of concentration gradients during the galvanostatic charge/ discharge process allows surface reactions to occur under near-equilibrium conditions.⁵² Figure 5 displays a GITT measurement of SIPE. Applying pulses of 15 s duration at 1 mA cm⁻² and with intermediate OCV steps of 180 s (240 repetitions) indeed yields a plateau of the voltage profile (contrary to the arc-like behaviour for the uninterrupted voltage profile), thus unambiguously evidencing rather poor Li+ diffusivity through the SEI ($D_{Li^+,SEI} \ll D_{Li^+,SIPE}$). Consequently, the SEI impairs Li+ ion transport in the whole system, as reflected by higher overvoltage at moderate and high current densities. Figure 6 schematically depicts this phenomenon. At low current densities (e.g. 0.05 mA cm⁻²⁾, Li⁺ ion movement takes place unhindered since Li+ diffusion through both electrolyte and SEI is sufficient to facilitate a rather constant Li+ concentration along the cell at low current density. At higher current densities, though, the low diffusivity of Li+ through the SEI limits the mass transport thus inevitably leading to local depletion of Li+ at one side and an apparent excess of Li⁺ at the other side of the cell. As Li⁺ ions are forced through the SEI during polarization, further EC decomposition favoured by high current densities and corresponding high cell voltages occurs, thereby deteriorating interfacial/interphasial reaction kinetics, yielding irreversible increases of the cell resistances R_{EI} + R_{SEI} and R_{CT} .

3.3 Investigation of SEI properties

To gain insights into SEI composition and draw correlations to the observed electrochemical processes during cell cycling, XPS spectra of cycled Li (both cathode and anode) after 5 and 30 cycles at a current density of 0.2 mA cm $^{-2}$ with 2 h stripping/plating duration and Li electrodes, which were in contact with the polymer membrane (assembled and disassembled after 24 h), were recorded (Figure 7). The SEI of all electrodes is mainly composed of carbonates (such as $\rm Li_2CO_3)$ and EC solvent decomposition products (MeOCO $_2\rm Li$ and EtOCO $_2\rm Li$), which can be clearly identified from the increase in the signal at 533.7 eV (0 1s spectra, Figure 7a) compared to pristine Lithium. 53

After being in contact with the polymer membrane as well as after cycling, less than 1 at% of both sulphur and nitrogen were detected by XPS (Figure 7b). Due to the absence of any additional peaks or changes of the peak position for both cycled and uncycled electrodes, the detected signals likely reflect residues due to contact of cell compounds or minor decomposition products of the SIPE generated in contact with

metallic Li rather than by electrochemical decomposition. In addition, small amounts of fluorine species (5 at%) LiF/CFx were detected, whereof CFx refers to decomposition products of PVdF-HFP.⁵⁴ The content of SEI compounds (at%) remains similar upon cycling, hence indicating that no continuous decomposition occurred. Moreover, no significant differences between anode and cathode were determined, while low standard deviations of the detected compounds at different spots on the Lithium metal electrodes imply rather homogenous SEI composition. Note, however, that the overall SEI composition is substantially different from common dual ion salt-based (liquid or solid) electrolytes where the SEI is dominated by decomposition products of the Lithium salt.^{29,31}

Here, the corresponding SEI of cycled Li|SIPE|Li electrodes is mainly composed of typical SEI compounds (such as $\text{Li}_2\text{CO}_3/\text{LiOH/carbonates}$) and EC decomposition products which are known to yield a dense SEI,²⁶ yet no further "anion" (SIPE) decomposition occurs.

However, studies demonstrate that high lithium salt concentrations reduce thickness and resistance of the resulting SEI layers, thus suppressing dendrite formation while improving the Coulombic efficiency upon cycling. 28,55 In case of a dry SIPE system, it was recently shown that addition of 2 wt% of a Lithium salt significantly decreases the interphase resistances while the SEI itself (thickness, composition etc.) was not investigated.⁵⁶ It was also emphasized that the SEI composition, porosity and thickness (significantly depending on the employed Lithium salt)^{29,57} influence the diffusivity of Li+ ions through the interphase and may be rate-limiting parameters.58 In the SIPE considered here, Li⁺ diffusion within the polymer membrane amounts $D_{Li^+} \approx 10^{-11} \text{ m}^2 \text{ s}^{-1}$, corresponding to an ionic conductivity of $\approx 10^{-3}$ S cm⁻¹, while there is common belief that ion transport in the SEI composed of these Li-containing compounds (Li₂CO₃/LiOH/Li₂O) primarily takes place along grain boundaries with D_{Li} + ranging from 10^{-14} to 10^{-16} m² s⁻¹ rather than through bulk grains. ^{59–61} In addition, the SEI thickness was estimated (based on ²⁹, explanation in the SI, Figure S6) to be >500 nm which is comparably thicker than reported SEI layers between 10 nm and 100 nm in case of reported Lithium salt based liquid and polymer electrolytes. 28,29,62 In good agreement with an occurrence of W_s in the impedance spectra, reflecting the presence of a blocking interfacial/interphasial layer, the structure and composition of the SEI obtained in case of SIPE appear to have less favourable Li+ transport characteristics. Thus, despite that immobilization of anions is in general a desirable electrolyte property, one should be aware of that a lack of anions as mobile species affects the chemistry and characteristics of the corresponding electrode|electrolyte interphases. In this context, also the discrepancies observed between theoretical and experimental J_{Lim} can be explained. Chazalviel's model (as well as most of the common models aiming at describing correlations between electrolyte properties and Li deposition behaviour) assumes ideal interphases with unlimited ionic transport,³⁸

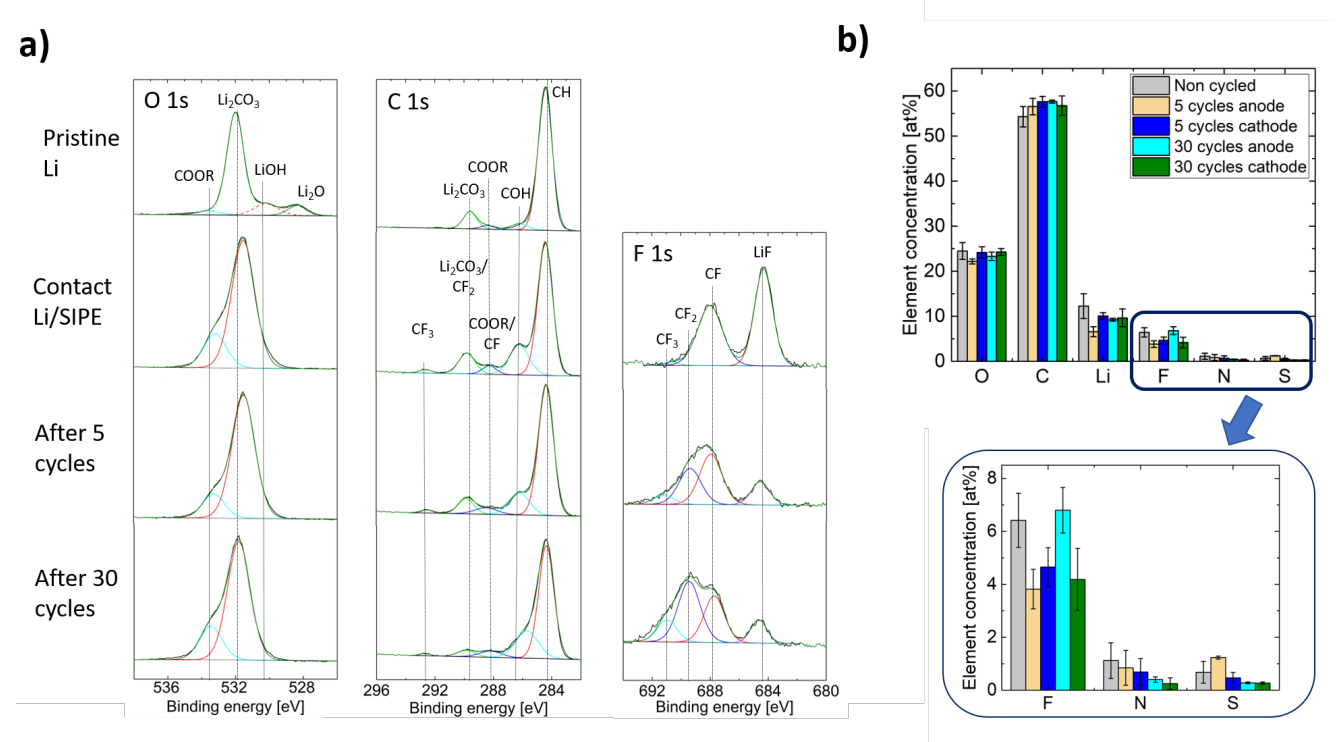


Figure 7 a) Fitted O 1s, C 1s and F 1s XPS spectra of the Li metal surface, Li after being in contact with SIPE (assembled and disassembled cell without cycling) and Li anodes after 5 and 30 cycles at 0.2 mA cm⁻² with 1 h stripping/plating duration and b) Mean element and compound concentration on the non-cycled and cycled (equal as in a)) electrodes.

which means that limitations of the electrolyte (not of the interphases) are reflected in this model. Therefore, unlike previously reported PEO/LiTFSI-based systems, where the polymer membranes limit the overall cell performance, affording consistency among theoretical and experimental J_{Lim} , it is highly plausible to observe cell failure below the expected value in case of the investigated SIPE since in this case interphasial properties are the major limiting factors within the cells.

Though this study was performed for a particular SIPE, the obtained insights are generally applicable to various electrolytes where interphase (both, SEI and cathode electrolyte interphase, CEI⁶³) properties constitute the 'bottleneck' for Li⁺ ion transport within the cells. This most likely affects the majority of SIPE (gel-type, quasi-solid or solid) where a lack of anions during the electrolyte decomposition process yields less favourable SEI/CEI transport properties as well as various ceramic or hybrid solid electrolytes where reduced interphase contact between electrolyte and electrode additionally contributes to a reduction of the interphasial Li⁺ ion transport.

For application of these electrolyte materials and to avoid polarization effects in SIPE, interphase or electrode design strategies or even combinations thereof are highly promising approaches to eventually tailor interphase compositions and characteristics, thereby enhancing the practically achievable J_{Lim} towards the materials' limitation. With respect to interphase engineering, incorporation of film forming additives in the electrolyte, even including addition of small amounts of Lithium salts, 56,64 or multi-layer attempts applying (single) Li⁺ ion conducting, flexible compounds maybe even in combination with

inorganic fillers⁶⁵ as artificial interphases represent viable strategies to achieve desired interphase chemistries and properties that prevent decomposition of the electrolyte or specific electrolyte compounds. In view of the SIPE considered here, the approaches for current investigations comprise application of artificial interphases by chemical pretreatment, e.g. of the Li anodes thereby incorporating inorganic moieties (e.g. F-, B-, P-, etc.) to layers as well as physical coating of Lithium with polymers (e.g. lithiated Nafion that was proposed as suitable interphase layer⁶⁶).

Beyond the design of the Li anode itself, including utilization of so called Li alloys that are less reactive towards the electrolyte and inhibit growth of high surface area Li deposits⁶⁷ or 3D host structures that accommodate Li metal and minimize volume changes of the electrode⁶⁸ and subsequently, continuous damage and reconstruction of the SEI (that in turn continuously consumes electrolyte compounds) might be a considered. A combinatorial approach, applying both, a lithium ion host material and an artificial SEI might be additionally considered to successfully address the issues of volumetric changes and surface protection of the anode simultaneously.

In this new perspective, the rational design and tailoring of interphases constitutes an additional challenge, which is at least as relevant as electrolyte development itself in terms of Lithium metal battery application. Rather than strictly focusing on the improvement of electrolyte transport properties (such as ionic conductivity, limiting current density or Li⁺ diffusivity) it is advocated to consider actual limitations of newly developed materials within a given cell system, eventually affording adaption of materials chemistry based on electrochemical processes at

electrode|electrolyte interfaces and interphases. Indeed, as exemplified here, complementary characterization techniques allow for elucidation of interphase properties and charge transfer mechanisms, thereby identifying likely kinetic 'bottlenecks' of a cell system, which then allows to determine suitable efficient strategies (either related to the electrolyte or the interphase) to further enhance overall cell performance.

CONCLUSION

In this contribution it is demonstrated that interphase characteristics can limit the ability of (single-ion conducting) polymer electrolytes for fast charging application. Comparison between theoretical and experimental limiting current density, J_{Lim} , of a SIPE are drawn where a discrepancy of both values is identified. Experimental stripping/plating experiments revealed that the application of moderate (0.5 mA cm⁻²) to high (1 mA cm⁻²) current densities unexpectedly yields an arcing of the overvoltage profiles related to polarization effects and a constant increase in overvoltage with increasing cycle. While there is no polarization expected in an ideal single-ion conductor with $t^+=1$, 'real' polymeric single- ion conducting electrolyte systems, e.g. due to minor decomposition reactions at the Li metal interphase or residual compounds within the actual polymer structure, exhibit t^+ <1. Thus, when applying an electric field, parasitic anionic currents are partially present and significantly influence the cell behaviour, particularly at higher current rates relevant in view of fast charging of cells (here, e.g., 0.5 mA cm⁻²).

Beyond that, a combinatorial approach involving various electrochemical and physiochemical methods revealed rather poor Li⁺ transport properties across a thick and predominately organic SEI (composed of decomposition products of plasticizers), rendering the bulk Li⁺ conductivity of SIPE less important for the lithium ion transport in the battery cell, i.e., overall cell performance. The SEI composition of SIPE will be inevitably affected by the lack of movable anions, as decomposition products of the anion are typical SEI components.²³As consequence, at high current densities, a Li⁺ ion concentration gradient is generated within the cell where Li⁺ ion transport through the anode interphase (SEI) can no longer compensate rather fast Li+ transport within the bulk electrolyte, eventually resulting in Li⁺ ion depletion at the positive electrode. In summary, even in case of SIPE-based systems, cell polarization occurs at sufficiently high current density, if $D_{Li^+,SEI} \ll D_{Li^+,SIPE}$. Consequently, since ideal interfaces/interphases are assumed in the framework of Chazalviel's model, the predicted $J_{Lim\ theo}$ cannot be reliably consulted for determination of system limitations, but rather the impact of actual interphases has to be included, as reflected by observed discrepancies between model-based and experimentally obtained values of J_{Lim} in case of SIPEs.

These findings provide insights into Li|SIPE interphase processes that have not yet been considered and that enable the development of unprecedented strategies such as specific interphase chemistry (SEI/CEI forming electrolyte additives or artificial SEI/CEI layers) and electrode compositions and designs (Li alloys or 3D host structures) or any combinations thereof to actually achieve improved electrochemical cell performance, even including long-term stability and establishment of fast

charging protocols (high current rates) necessary in view of industrial applications.

ASSOCIATED CONTENT

Supporting Information

The Supporting Information is available free of charge on the ACS Publications website.

Voltage profiles of a i|SIPE|Li stripping/plating experiment in Figure 1b, Voltage profile of a stripping/plating experiment of a polymer membrane composed of 1:1 (wt%: wt%) single ion-conducting polymer: PVdF-HFP, ¹H NMR and FTIR spectra of fresh and cycled membranes, Stripping/plating and OCV of a second Li|SIPE|Li, Explanation and demonstration of the determination of SEI thickness based on EIS spectra (PDF)

AUTHOR INFORMATION

Corresponding Author

*g.brunklaus@fz-juelich.de

Author Contributions

Concept, K.B., J.N.; Methodology, K.B., G.B.; Writing – Original Draft, K.B.; Writing – Review & Editing J.N., G.B. and M.W., Supervision, G.B., M.W.

ACKNOWLEDGMENT

The authors gratefully acknowledge generous support provided by the German Federal Ministry of Education and Research (BMBF) projects 'Festbatt' (grant 13XP0175A) and 'Benchbatt' (03XP0047B).

REFERENCES

- (1) Placke, T.; Kloepsch, R.; Dühnen, S.; Winter, M. Lithium Ion, Lithium Metal, and Alternative Rechargeable Battery Technologies: The Odyssey for High Energy Density. J. Solid State Electrochem. 2017, 21 (7), 1939–1964.
- (2) Schmuch, R.; Wagner, R.; Hörpel, G.; Placke, T.; Winter, M. Performance and Cost of Materials for Lithium-Based Rechargeable Automotive Batteries. *Nat. Energy* **2018**, *3* (4), 267–278.
- (3) Shen, X.; Liu, H.; Cheng, X. B.; Yan, C.; Huang, J. Q. Beyond Lithium Ion Batteries: Higher Energy Density Battery Systems Based on Lithium Metal Anodes. *Energy Storage Mater.* **2018**, *12* (November 2017), 161–175.
- (4) Winter, M.; Barnett, B.; Xu, K. Before Li Ion Batteries. *Chem. Rev.* **2018**, *118* (23), 11433–11456.
- (5) Nair, J. R.; Imholt, L.; Brunklaus, G.; Winter, M. Lithium Metal Polymer Electrolyte Batteries: Opportunities and Challenges. Electrochem. Soc. Interface 2019, 28 (2), 55–61.
- (6) Mindemark, J.; Lacey, M. J.; Bowden, T.; Brandell, D. Beyond PEO—Alternative Host Materials for Li + -Conducting Solid Polymer Electrolytes. *Prog. Polym. Sci.* 2018, 81, 114–143.
- (7) Long, L.; Wang, S.; Xiao, M.; Meng, Y. Polymer Electrolytes for Lithium Polymer Batteries. J. Mater. Chem. A 2016, 4 (26), 10038–10069.
- (8) Chazalviel, J.-N. Electrochemical Aspects of the Generation of Ramified Metallic Electrodeposits. *Phys. Rev. A* 1990, 42 (12), 7355–7367.
- (9) Brissot, C.; Rosso, M.; Chazalviel, J. N.; Lascaud, S. In Situ Concentration Cartography in the Neighborhood of Dendrites Growing in Lithium/Polymer-Electrolyte/Lithium Cells. J. Electrochem. Soc. 1999, 146 (12), 4393–4400.

- (10) Laoire, C. O.; Plichta, E.; Hendrickson, M.; Mukerjee, S.; Abraham, K. M. Electrochemical Studies of Ferrocene in a Lithium Ion Conducting Organic Carbonate Electrolyte. Electrochim. Acta 2009, 54 (26), 6560–6564.
- (11) Lee, S. I.; Jung, U. H.; Kim, Y. S.; Kim, M. H.; Ahn, D. J.; Chun, H. S. A Study of Electrochemical Kinetics of Lithium Ion in Organic Electrolytes. *Korean J. Chem. Eng.* 2002, 19 (4), 638– 644.
- (12) Park, J. W.; Yoshida, K.; Tachikawa, N.; Dokko, K.; Watanabe, M. Limiting Current Density in Bis(Trifluoromethylsulfonyl)Amide-Based Ionic Liquid for Lithium Batteries. J. Power Sources 2011, 196 (4), 2264–2268.
- (13) Gribble, D. A.; Frenck, L.; Shah, D. B.; Maslyn, J. A.; Loo, W. S.; Mongcopa, K. I. S.; Pesko, D. M.; Balsara, N. P. Comparing Experimental Measurements of Limiting Current in Polymer Electrolytes with Theoretical Predictions. *J. Electrochem. Soc.* 2019, 166 (14), A3228–A3234.
- (14) Ma, Q.; Zhang, H.; Zhou, C.; Zheng, L.; Cheng, P.; Nie, J.; Feng, W.; Hu, Y.-S. S.; Li, H.; Huang, X.; Chen, L.; Armand, M.; Zhou, Z. Single Lithium-Ion Conducting Polymer Electrolytes Based on a Super-Delocalized Polyanion. *Angew. Chemie Int. Ed.* 2016, 128 (7), 2521–2525.
- (15) Zhang, H.; Li, C.; Piszcz, M.; Coya, E.; Rojo, T.; Rodriguez-Martinez, L. M.; Armand, M.; Zhou, Z. Single Lithium-Ion Conducting Solid Polymer Electrolytes: Advances and Perspectives. Chem. Soc. Rev. 2017, 46 (3), 797–815.
- (16) Deng, K.; Zeng, Q.; Wang, D.; Liu, Z.; Qiu, Z.; Zhang, Y.; Xiao, M.; Meng, Y. Single-Ion Conducting Gel Polymer Electrolytes: Design, Preparation and Application. *J. Mater. Chem.* **2020**, *8* (4), 1557–1577.
- (17) Jeong, K.; Park, S.; Lee, S. Y. Revisiting Polymeric Single Lithium-Ion Conductors as an Organic Route for All-Solid-State Lithium Ion and Metal Batteries. J. Mater. Chem. A 2019, 7 (5), 1917–1935.
- (18) Zhu, J.; Zhang, Z.; Zhao, S.; Westover, A. S.; Belharouak, I.; Cao, P. Single-Ion Conducting Polymer Electrolytes for Solid-State Lithium Metal Batteries: Design, Performance, and Challenges. Adv. Energy Mater. 2021, 2003836.
- (19) Gan, H.; Zhang, Y.; Li, S.; Yu, L.; Wang, J.; Xue, Z. Self-Healing Single-Ion Conducting Polymer Electrolyte Formed via Supramolecular Networks for Lithium Metal Batteries. ACS Appl. Energy Mater. 2020, 4 (1), 482–491.
- (20) Krause, C. H.; Butzelaar, A. J.; Diddens, D.; Dong, D.; Theato, P.; Bedrov, D.; Hwang, B.-J.; Winter, M.; Brunklaus, G. Quasi-Solid Single Ion Conducting Polymer Electrolyte Membrane Containing Novel Fluorinated Poly(Arylene Ether Sulfonimide) for Lithium Metal Batteries. J. Power Sources 2021, 484, 229267.
- (21) Stolz, L.; Homann, G.; Winter, M.; Kasnatscheew, J. Kinetical Threshold Limits in Solid-State Lithium Batteries: Data on Practical Relevance of Sand Equation. *Data Br.* 2021, 34, 106688
- (22) Winter, M. The Solid Electrolyte Interphase-The Most Important and the Least Understood Solid Electrolyte in Rechargeable Li Batteries. Zeitschrift für Phys. Chemie 2009, 223 (10–11), 1395– 1406
- (23) Niehoff, P.; Passerini, S.; Winter, M. Interface Investigations of a Commercial Lithium Ion Battery Graphite Anode Material by Sputter Depth Profile X-Ray Photoelectron Spectroscopy. *Langmuir* **2013**, *29* (19), 5806–5816.
- (24) Wood, K. N.; Teeter, G. XPS on Li-Battery-Related Compounds: Analysis of Inorganic SEI Phases and a Methodology for Charge Correction. ACS Appl. Energy Mater. 2018, 1 (9), 4493–4504.
- (25) Fiedler, C.; Luerssen, B.; Rohnke, M.; Sann, J.; Janek, J. XPS and SIMS Analysis of Solid Electrolyte Interphases on Lithium Formed by Ether-Based Electrolytes. J. Electrochem. Soc. 2017, 164 (14), A3742–A3749.
- (26) Cheng, X. B.; Zhang, R.; Zhao, C. Z.; Wei, F.; Zhang, J. G.; Zhang, Q. A Review of Solid Electrolyte Interphases on Lithium Metal Anode. Adv. Sci. 2015, 3 (3), 1–20.
- (27) Cheng, X. B.; Zhang, R.; Zhao, C. Z.; Zhang, Q. Toward Safe Lithium Metal Anode in Rechargeable Batteries: A Review. Chem. Rev. 2017, 117 (15), 10403–10473.
- (28) Jeong, S. K.; Seo, H. Y.; Kim, D. H.; Han, H. K.; Kim, J. G.; Lee,

- Y. B.; Iriyama, Y.; Abe, T.; Ogumi, Z. Suppression of Dendritic Lithium Formation by Using Concentrated Electrolyte Solutions. *Electrochem. commun.* **2008**, *10* (4), 635–638.
- (29) Ismail, I.; Noda, A.; Nishimoto, A.; Watanabe, M. XPS Study of Lithium Surface after Contact with Lithium-Salt Doped Polymer Electrolytes. *Electrochim. Acta* 2001, 46 (10–11), 1595–1603.
- (30) Qian, J.; Henderson, W. A.; Xu, W.; Bhattacharya, P.; Engelhard, M.; Borodin, O.; Zhang, J. G. High Rate and Stable Cycling of Lithium Metal Anode. *Nat. Commun.* 2015, 6.
- (31) Xu, C.; Sun, B.; Gustafsson, T.; Edström, K.; Brandell, D.; Hahlin, M. Interface Layer Formation in Solid Polymer Electrolyte Lithium Batteries: An XPS Study. J. Mater. Chem. A 2014, 2 (20), 7256–7264.
- (32) Nölle, R.; Beltrop, K.; Holtstiege, F.; Kasnatscheew, J.; Placke, T.; Winter, M. A Reality Check and Tutorial on Electrochemical Characterization of Battery Cell Materials: How to Choose the Appropriate Cell Setup. *Mater. Today* **2020**, *32*, 131-146.
- (33) Borzutzki, K.; Thienenkamp, J.; Diehl, M.; Winter, M.; Brunklaus, G. Fluorinated Polysulfonamide Based Single Ion Conducting Room Temperature Applicable Gel-Type Polymer Electrolytes for Lithium Ion Batteries. *J. Mater. Chem. A* **2019**, 7 (1), 188–201.
- (34) Becking, J.; Gröbmeyer, A.; Kolek, M.; Rodehorst, U.; Schulze, S.; Winter, M.; Bieker, P.; Stan, M. C. Lithium-Metal Foil Surface Modification: An Effective Method to Improve the Cycling Performance of Lithium-Metal Batteries. Adv. Mater. Interfaces 2017, 4 (16), 1700166.
- (35) Betz, J.; Brinkmann, J. P.; Nölle, R.; Lürenbaum, C.; Kolek, M.; Stan, M. C.; Winter, M.; Placke, T. Cross Talk between Transition Metal Cathode and Li Metal Anode: Unraveling Its Influence on the Deposition/Dissolution Behavior and Morphology of Lithium. Adv. Energy Mater. 2019, 9 (21), 1–10.
- (36) Borzutzki, K.; Winter, M.; Brunklaus, G. Improving the NMC111|polymer Electrolyte Interface by Cathode Composition and Processing. *J. Electrochem. Soc.* **2020**, *167* (7), 070546.
- (37) Borzutzki, K.; Dong, D.; Wölke, C.; Kruteva, M.; Stellhorn, A.; Winter, M.; Bedrov, D.; Brunklaus, G. Small Groups, Big Impact: Eliminating Li+ Traps in Single-Ion Conducting Polymer Electrolytes. *iScience* **2020**, *23* (8), 101417.
- (38) Brissot, C.; Rosso, M.; Chazalviel, J.-N.; Lascaud, S. Dendritic Growth Mechanisms in Lithium/Polymer Cells. *J. Power Sources* **1999**, *81–82* (81–82), 925–929.
- (39) Ford, H.; Park, B.; Jiang, J.; Schaefer, J. Enhanced Li+ Conduction Within Single-Ion Conducting Crosslinked Gel via Reduced Cation-Polymer Interaction. ACS Mater. Lett. 2019, 2, 272–279
- (40) Nguyen, H.-D.; Kim, G.-T.; Shi, J.; Paillard, E.; Judenstein, P.; Lyonnard, S.; Bresser, D.; Iojoiu, C. Nanostructured Multi-Block Copolymer Single-Ion Conductors for Safer High-Performance Lithium Batteries. *Energy Environ. Sci.* 2018, 11 (11), 3298–3309.
- (41) Rosso, M.; Gobron, T.; Brissot, C.; Chazalviel, J. N.; Lascaud, S. Onset of Dendritic Growth in Lithium/Polymer Cells. J. Power Sources 2001, 97–98, 804–806.
- (42) Tasaki, K. Solvent Decompositions and Physical Properties of Decomposition Compounds in Li-Ion Battery Electrolytes Studied by DFT Calculations and Molecular Dynamics Simulations. J. Phys. Chem. B 2005, 109 (7), 2920–2933.
- (43) Bieker, G.; Winter, M.; Bieker, P. Electrochemical in Situ Investigations of SEI and Dendrite Formation on the Lithium Metal Anode. *Phys. Chem. Chem. Phys.* 2015, 17 (14), 8670– 8679.
- (44) Su, Y.; Ye, L.; Fitzhugh, W.; Wang, Y.; Gil-González, E.; Kim, I.; Li, X. A More Stable Lithium Anode by Mechanical Constriction for Solid State Batteries. *Energy Environ. Sci.* 2020, 13 (3), 908–916.
- (45) Liu, K.; Li, X.; Cai, J.; Yang, Z.; Chen, Z.; Key, B.; Zhang, Z.; Dzwiniel, T. L.; Liao, C. Design of High-Voltage Stable Hybrid Electrolyte with an Ultrahigh Li Transference Number. ACS Energy Lett. 2021, 1315–1323.
- (46) Yuan, X.-Z.; Song, C.; Wang, H.; Zhang, J. Electrochemical Impedance Spectroscopy in PEM Fuel Cells: Fundamentals and Applications; Springer Science & Business Media, 2009.

- (47) Single, F.; Horstmann, B.; Latz, A. Theory of Impedance Spectroscopy for Lithium Batteries. *J. Phys. Chem. C* **2019**, *123* (45), 27327–27343.
- (48) Evans, J.; Vincent, C. A.; Bruce, P. G. Electrochemical Measurement of Transference Number in Polymer Electrolytes. *Polymer*, 1987, 28 (13), 2324–2328.
- (49) Weppner, W.; Huggins, R. A. Determination of the Kinetic Parameters of Mixed-Conducting Electrodes and Application to the System Li3Sb. J. Electrochem. Soc. 1977, 124 (10), 1569– 1578.
- (50) Deiss, E. Spurious Chemical Diffusion Coefficients of Li+ in Electrode Materials Evaluated with GITT. *Electrochim. Acta* 2005, 50 (14), 2927–2932.
- (51) Yuan, X.; Ma, Z. F.; Nuli, Y.; Xu, N. Study on Hydrogen Diffusion Behavior in AB5-Type Hydrogen Storage Alloys with Galvanostatic Intermittent Titration Technique (GITT). J. Alloys Compd. 2004, 385 (1–2), 90–95.
- (52) Chen, K. H.; Wood, K. N.; Kazyak, E.; Lepage, W. S.; Davis, A. L.; Sanchez, A. J.; Dasgupta, N. P. Dead Lithium: Mass Transport Effects on Voltage, Capacity, and Failure of Lithium Metal Anodes. J. Mater. Chem. A 2017, 5 (23), 11671–11681.
- (53) Dedryvère, R.; Gireaud, L.; Grugeon, S.; Laruelle, S.; Tarascon, J. M.; Gonbeau, D. Characterization of Lithium Alkyl Carbonates by X-Ray Photoelectron Spectroscopy: Experimental and Theoretical Study. J. Phys. Chem. B 2005, 109 (33), 15868–15875.
- (54) Manuel Stephan, A.; Nahm, K. S. Review on Composite Polymer Electrolytes for Lithium Batteries. *Polyme* 2006, 47 (16), 5952– 5964
- (55) Yamaki, J.; Tobishima, S. Rechargeable Lithium Anodes. In Handbook of battery materials; WILEY-VCH Verlag GmbH, 1999; pp 339–375.
- (56) Martinez-Ibañez, M.; Sanchez-Diez, E.; Qiao, L.; Zhang, Y.; Judez, X.; Santiago, A.; Aldalur, I.; Carrasco, J.; Zhu, H.; Forsyth, M.; Armand, M.; Zhang, H. Unprecedented Improvement of Single Li-Ion Conductive Solid Polymer Electrolyte Through Salt Additive. Adv. Funct. Mater. 2020, n/a (n/a), 2000455.
- (57) Aurbach, D.; Weissman, I.; Zaban, A.; Chusid, O. Correlation between Surface Chemistry, Morphology, Cycling Efficiency and Interfacial Properties of Li Electrodes in Solutions Containing Different Li Salts. *Electrochim. Acta* 1994, 39 (1), 51–71.
- (58) Li, Y.; Leung, K.; Qi, Y. Computational Exploration of the Li-Electrode|Electrolyte Interface in the Presence of a Nanometer

- Thick Solid-Electrolyte Interphase Layer. Acc. Chem. Res. 2016, 49 (10), 2363–2370.
- (59) Ramasubramanian, A.; Yurkiv, V.; Foroozan, T.; Ragone, M.; Shahbazian-Yassar, R.; Mashayek, F. Lithium Diffusion Mechanism through Solid-Electrolyte Interphase in Rechargeable Lithium Batteries. J. Phys. Chem. C 2019, 123 (16), 10237– 10245.
- (60) Shi, S.; Qi, Y.; Li, H.; Hector, L. G. Defect Thermodynamics and Diffusion Mechanisms in Li2CO 3 and Implications for the Solid Electrolyte Interphase in Li-Ion Batteries. J. Phys. Chem. C 2013, 117 (17), 8579–8593.
- (61) Chen, Y. C.; Ouyang, C. Y.; Song, L. J.; Sun, Z. L. Electrical and Lithium Ion Dynamics in Three Main Components of Solid Electrolyte Interphase from Density Functional Theory Study. J. Phys. Chem. C 2011, 115 (14), 7044–7049.
- (62) Peled, E.; Menkin, S. Review SEI: Past, Present and Future. J. Electrochem. Soc. 2017, 164 (7), A1703–A1719.
- (63) Gallus, D. R.; Wagner, R.; Wiemers-Meyer, S.; Winter, M.; Cekic-Laskovic, I. New Insights into the Structure-Property Relationship of High-Voltage Electrolyte Components for Lithium-Ion Batteries Using the PKa Value. *Electrochim. Acta* 2015, 184, 410–416.
- (64) Cekic-Laskovic, I.; von Aspern, N.; Imholt, L.; Kaymaksiz, S.; Oldiges, K.; Rad, B. R.; Winter, M. Synergistic Effect of Blended Components in Nonaqueous Electrolytes for Lithium Ion Batteries. *Top. Curr. Chem.* 2017, 375 (2), 1–64.
- (65) Wu, C.; Guo, F.; Zhuang, L.; Ai, X.; Zhong, F.; Yang, H.; Qian, J. Mesoporous Silica Reinforced Hybrid Polymer Artificial Layer for High-Energy and Long-Cycling Lithium Metal Batteries. ACS Energy Lett. 2020, 5 (5), 1644–1652.
- (66) Tu, Z.; Choudhury, S.; Zachman, M. J.; Wei, S.; Zhang, K.; Kourkoutis, L. F.; Archer, L. A. Designing Artificial Solid-Electrolyte Interphases for Single-Ion and High-Efficiency Transport in Batteries. *Joule* 2017, 1 (2), 394–406.
- (67) Yang, X.; Peng, Y.; Hou, J.; Liu, Y.; Jian, X. A Review for Modified Li Composite Anode: Principle, Preparation and Challenge. *Nanotechnol. Rev.* 2020, 9 (1), 1610–1624.
- (68) Wang, H.; Liu, Y.; Li, Y.; Cui, Y. Lithium Metal Anode Materials Design: Interphase and Host. *Electrochem. Energy Rev.* 2019, 2 (4), 509–517.

Table of Contents artwork

